Aerospace Science and Technology 58 (2016) 48–59

Contents lists available at ScienceDirect

Aerospace Science and Technology

www.elsevier.com/locate/aescte

Rapid prediction of hypersonic blunt body flows for parametric design studies

W. Schuyler Hinman *, Craig T. Johansen

ARTICLE INFO

Article history:
Received 9 May 2016
Received in revised form 3 August 2016
Accepted 4 August 2016
Available online 10 August 2016

ABSTRACT

The present work discusses the practical advantages and disadvantages of using simplified numerical methods and computational fluid dynamics in parametric design studies of hypersonic blunt bodies. Similarly, the advantages of using problem-specific simplifications to the governing equations to reduce computational cost are discussed. The uncertainty associated with using various methods to analyze hypersonic blunt body flows has been quantified through comparison to numerical solutions of the compressible Navier–Stokes equations. In particular, selected methods that are well defined in the literature, such as the modified Newtonian method, transformed finite difference grids, and the method of characteristics in the supersonic region, have been utilized to solve two cases of interest. An improvement to the prediction methods has been achieved through the inclusion of an iterative interaction between the boundary layer displacement thickness and the external inviscid free-stream. Results were collected for accuracy and computing time for each method including under-resolved compressible Navier–Stokes simulations. The collective information was used as a case-study to discuss the balance an engineer must find between simulation fidelity, resolution, accuracy, simulation time, and development time.

1. Introduction

The design of hypersonic blunt-body vehicles requires accurate predictions of aerodynamic loads such as drag, friction, moments, and heat flux. In general, computational fluid dynamics (CFD) simulations of the Navier–Stokes equations provide the most accurate and detailed predictions of these flow parameters. The highly accurate results of Navier–Stokes simulations are particularly useful when a vehicle geometry is past the initial design phase and more accurate predictions are needed to optimize re-entry trajectory, heating or placement of control mechanisms. However, in the ongoing advancement and development of blunted hypersonic geometries, the shape of the body may be further improved upon through parametric studies and optimizations [1–3]. These types of studies involve evaluating many design variables. In these cases, where the best results are achieved with large populations, CFD is an inefficient prediction tool due to the high computational cost. Often a compromise is made in grid resolution, and hence accuracy, in order to keep a parametric or optimization study feasible [4]. It is unclear whether such a reduction in resolution in order to reduce computing time, while maintaining the highest fidelity governing equations, is the appropriate strategy. Alternatively, the governing equations themselves can be simplified and solved with high resolution in order to achieve a reduction in computing time, provided that some prior wisdom of the problem exists. Both of these approaches result in decreased accuracy either by a lack of resolution, or from simplifications to the governing equations. A major problem in starting an analysis or optimization campaign is “how does the designer/engineer/scientist choose the correct tool?”. In flow prediction, the engineer must weigh all of the costs of available tools against their value in terms of speed, reliability and accuracy. Obvious costs include the acquisition/development costs and the operational costs. However, the learning curve associated with a new tool is also an important cost. These decisions are often made based on previous experiences and expertise. The purpose of this work is to assist with making that decision by systematically assessing the accuracy and cost of a range of analysis methods used in hypersonic flow prediction. Assessment is based on the prediction of a complex, but well-known, canonical flow problem. Hypersonic flow over a cylinder involves regions that are described by elliptic, parabolic, and hyperbolic equations. Large changes in temperature require proper treatment of the thermophysical properties. The presence of shock waves introduce discontinuities that compromise accuracy, lead to instability, and increase computing time for most standard numerical methods. The present work has attempted to examine this problem by comparing a series of blunt body flow calculations of varying fidelity. The study includes two test cases: (1) a Mach 6, two-dimensional, laminar flow over a circular cylinder with an

* Corresponding author.
E-mail address: wshinman@ucalgary.ca (W.S. Hinman).

http://dx.doi.org/10.1016/j.ast.2016.08.007
1270-9638/

Nomenclature

a	Velocity profile parameter (in Equation (6) and (7)), also speed of sound (m/s)
b	Body shape, measured radially from the origin (m)
As	Sutherland constant
C	$C = \frac{\rho\mu}{\rho_e\mu_e}$
C_p	Coefficient of pressure
C_1, C_2, C_3	Coefficients for Kays' laminar heating (in Equation (3))
c_p	Specific heat capacity J/(kg K)
c_f	Coefficient of friction
F	$F = \frac{U}{U_e}$
G	$G = \frac{H}{H_e}$
G_e	$\rho_e U_e$ (in Equation (3))
H	Total enthalpy (J/kg)
H, J, R, P	Boundary layer integral parameters (in Equations (6) and (7))
m	Displacement thickness growth ($\frac{d\delta^\star}{dx}$)
M	Mach number
p	Pressure (Pa)
q_∞	Free-stream dynamic pressure (Pa)
Pr	Prandtl number
r	Adiabatic recovery factor (in Equation (20)), also relaxation factor (in Equation (26))
R	Local axi-symmetric radius of curvature (m) (in Equation (3))
R_g	Specific gas constant J/(kg K)
Re	Reynolds number
Re_c	Cell Reynolds number
$\bar{s}$	Levy–Lees stream-wise coordinate
T	Temperature (K)
T_{aw}	Adiabatic wall temperature (K)
T_s	Sutherland's temperature (K)
u	Velocity vector (m/s)
U	Tangent velocity component (m/s) (boundary layer equations)
V	Normal velocity component (m/s) (boundary layer equations)
X	Stewartson stream-wise coordinate
Y	Stewartson stream-normal coordinate
γ	Specific heat ratio
δ^*	Boundary layer displacement thickness (m)
η	Levy–Lees stream-normal coordinate
θ	Deflection angle (radians or degrees)
μ	Dynamic viscosity (kg/ms)
ρ	Density (kg/m^3)
τ	Shear stress (N/m^2)

Subscript

e	Property at boundary layer edge
i	Transformed quantity, also iteration
o	Property at forward stagnation point
w	Property at wall
∞	Free-stream property

adiabatic wall, not including the separated wake region, and (2) a Mach 10, two-dimensional, laminar flow over a blunted leading edge with a cold wall.

Parametric studies and design optimizations are a fundamental tool in the development of future aerospace technologies. In CFD applications these types of studies can be very expensive due to the high computational requirements of the governing Navier–Stokes equations. Because of this there is interest in finding ways to reduce this cost with minimal compromise in accuracy and confidence. For example, surrogate based analyses are very common in CFD applications because they do not require a Navier–Stokes simulation to be performed at every data point. Instead, a surrogate model uses data achieved through high fidelity simulations performed at select points in the design space to create a model [5]. Additionally, surrogate models can be constructed using a combination of high and low fidelity simulations [6,7]. This leads to a significantly reduced cost of performing parametric optimizations and analyses. However, even in a surrogate-model based study, a complicated design space can still require numerous high-fidelity simulations to be performed. Additionally, it is important to understand the limitations and benefits of using intermediate fidelity approaches. For this reason there is still value in reducing the cost of individual simulations. It is easy to assume that high-fidelity CFD is required in order to produce the level of accuracy necessary in modern design. While in some cases this is true, in others it is worth investigating the possible reduced-order and simplified models that have been developed and used in the past. For example, in previous work by the present authors, simplified numerical solutions were used with a genetic algorithm to optimize wave-rider leading edges [1]. The reduced-order model allowed a large number of simulations to be performed with high accuracy. The optimized results were then examined using high-fidelity CFD and it was found that the predicted performance gains from the optimization were not significantly in error. Because of the speed and accuracy of the models used, no surrogate based modeling was required.

Many simplified solutions to flow over hypersonic blunt bodies exist. A representative few are presented here in order to provide the necessary data for analysis and discussion. Two methods of varying accuracy for inviscid flow have been examined: (1) The modified Newtonian method [8] and (2) a numerical solution to the Euler equations using finite differences [8,9] combined with the method of characteristics [8,10]. Similarly, several methods for producing boundary-layer flow solutions are examined: (1) A simple solution for convective heat flux described by Kays et al. [11], (2) a solution to the integral boundary layer equations using the Cohen–Reshotko family of profiles [12,13], and (3) a direct numerical solution of the complete compressible boundary layer equations [14]. Each of these methods are solved in combination with each other to achieve a representative variation in accuracy. These methods are described in more detail in Section 2. Because flowfields of practical interest are a mixture of viscous and inviscid flow it is often necessary to account for viscous-inviscid interaction. In the case a circular cylinder an interaction occurs between the shoulder expansion fan and the boundary layer flow. A simple iterative algorithm to account for this interaction is presented in Section 3.

For the solution of the compressible Navier–Stokes equations the open source CFD package OpenFOAM version 2.3.0 was used [15]. The solver used in this work, rhoCentralFoam, has been compared to experiment as well as other solvers from other CFD packages and shown acceptable results [16–19]. Arisman et al. [17,18] used a modified form of the rhoCentralFOAM solver to compute the injection of nitric oxide in a cross-flow configuration into a Mach 10 boundary layer with air as the freestream. Vertical distributions of predicted streamwise velocity were compared to experimental planar laser-induced fluorescence (PLIF) molecular tagging velocimetry (MTV) measurements. In addition to velocity, a surface

pressure probe was used to capture the hypersonic viscous interaction at the leading edge of the wind-tunnel model. The estimated error of the simulations based on comparisons of velocity and pressure were 2% and 3%, respectively. Hinman and Johansen [16] used rhoCentralFoam to study the present case of hypersonic flow over an adiabatic circular cylinder. The computational results in that work were compared to experimental base pressure measurements by McCarthy and Kubota [20]. In the cases compared, the computational results for base pressure distribution had a maximum error of 0.65% of stagnation pressure from the experimental values. This is slightly larger than the estimated experimental error for these data points ($\pm$ 0.2% of stagnation pressure). This additional error was attributed to uncertainty in matching the nominal Reynolds and Mach numbers from the experiments. At higher relative Reynolds number (where this uncertainty has less effect) the maximum error was only 0.12% of stagnation pressure. Very close to the reported experimental uncertainty of $\pm$ 0.1% of stagnation pressure for these cases. Because of these previous successes, the present authors are comfortable using rhoCentralFoam as the benchmark for accuracy in the current work.

The discussion in this study should be useful to engineers performing parametric design studies on two dimensional or axisymmetric hypersonic blunt body geometries such as launch vehicles, high-speed aircraft, projectiles, missiles, or atmospheric entry systems. More generally, this work serves as an example of the balance that must be struck between fidelity, resolution, accuracy and simulation time.

2. Description of numerical and mathematical models

2.1. Summary

In order to provide insight into the benefits of using reduced fidelity models in parametric design studies of hypersonic flow, a number of methods were implemented. These ranged from low fidelity to high fidelity. None of the individual methods for solving inviscid or viscous presented here are themselves novel and can be found described in significant detail in the literature. The reduced fidelity models in this paper are outlined in Table 1. In Sections 2.2 to 2.4 the low and intermediate fidelity approaches are briefly described. In Section 3 the viscous-inviscid coupling algorithm used for the a region of expansion is outlined. In Section 4 the CFD set-up for the compressible Navier–Stokes simulations is described briefly. For detailed explanations of the implementations of these methods, the references from Table 1 should be consulted. In this study these methods have only been applied for two-dimensional flows. However, this does not mean that these methods are incapable of analyzing more complicated geometries. For example, all of these methods can be modified for axisymmetric body geometries. Axisymmetric results have not been presented here because they are currently not a focus of the associated research and development projects of the authors. Fully three-dimensional bodies (such as a re-entry vehicle at an angle of attack) can often be analyzed by low fidelity methods, however achieving intermediate fidelity for these complicated flow-fields becomes much more complicated and difficult.

2.2. Inviscid flow

2.2.1. Local surface inclination methods (Newtonian method)

The simplest inviscid solutions to the supersonic compressible flow fields near surfaces are the local surface inclination methods. The modified Newtonian method is derived based on Newtonian impact theory and is given in Equation (1). The pressure coefficient utilized in the method is defined in Equation (2). $C_{p_{max}}$ is calculated using the post shock stagnation pressure with Equation (2). θ is the deflection angle from the incoming free-stream flow.

Table 1
Summary of flow-field solution methods.

Flow assumption/ solution type	Method	Fidelity	References
Inviscid Flow	Newtonian Impact Theory	Low	[8]
	Shock-Fitted Finite Difference Grid	Intermediate	[8,9]
	Method of Characteristics	Intermediate	[8,10]
Viscous Flow and Heating	Kays et al. [11] Laminar Heating	Low	[11]
	Integral Boundary Layer	Intermediate	[14,12,21,22,13]
	Numerical Boundary Layer	Intermediate	[14,21]
Coupled Solution	Viscous-Inviscid Coupling	Intermediate	[21,22]
Compressible Navier–Stokes Equations	rhoCentralFoam	High	[15]

$$C_p = C_{p_{max}} \sin^2 \theta \tag{1}$$

$$C_p = \frac{p - p_\infty}{\frac{1}{2}\rho_\infty V_\infty^2} \tag{2}$$

A major disadvantage of the Newtonian method is that past a deflection angle of 0 degrees (such as on a projectile aft-body), it is assumed that the pressure coefficient $C_p = 0$. This means that the pressure is assumed to be equal to the free-stream value (see Equation (2)). Unfortunately, this limits the applicability of the Newtonian method to flows where the deflection angle is small.

2.2.2. Shock-fitted finite difference grid (elliptic Euler equations)

On the forebody of the blunt body, the flow is subsonic and the governing Euler equations are elliptic in nature. The governing equations in this region can be solved through a time-stepping, shock-fitted, transformed finite difference grid for both two-dimensional and axisymmetric geometries [8,9]. In standard finite volume solutions the grid extends across shock waves, and complicated numerical techniques are required in order to accurately capture the steep gradients in flow properties. By utilizing shock-fitting techniques, the boundaries of the computational grid are limited to the fore-body region. This significantly reduces the computation time by reducing mesh size, and speeds convergence by avoiding complicated shock capturing techniques. The method as explained by both Salas [9] (in cylindrical coordinates), and Anderson [8] (in Cartesian coordinates), utilizes a transformed grid between the shock-wave shape and the body. The use of the transformed finite difference grid is attractive because any arbitrary body that can be represented by an equation or set of points can be transformed to a rectangular grid. This also becomes an asset in the proposed viscous-inviscid interaction scheme. The basics of this method, as well as the formulation of the transformed governing equations are described in detail by Salas and Anderson [9,8].

The shock fitted finite difference method (SFFD) was adapted directly from the sample code provided in the book by Salas [9]. Slight modifications were made to the code to implement thermophysical modelling of gas properties (see Section 2.4), and for the curve-fit geometries utilized in the viscous correction. The code has also been modified to perform 2D simulations with no symmetry plane [1]. A typical finite difference grid is shown in Fig. 1. The grid extends from the shock wave to the body, and from the symmetry plane to the outlet boundary. In a case with no symmetry plane the grid extends from lower outlet boundary to upper outlet boundary. The problem is initialized by assuming a shape for the shock [9]. The quality of this initial guess is important because if the shape is significantly in error, the solution convergence will

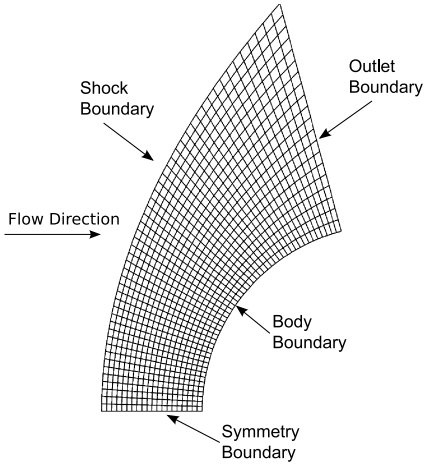

Fig. 1. Typical shock-fitted finite difference grid.

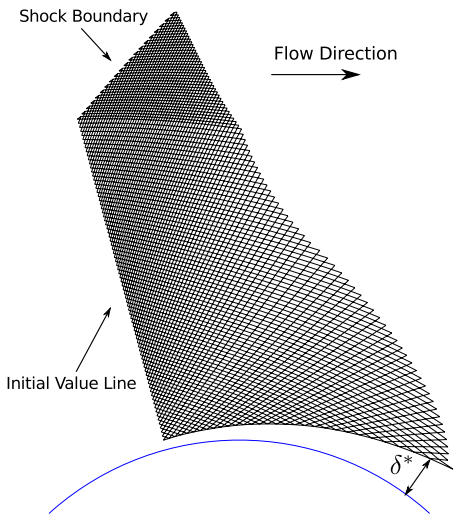

Fig. 2. Typical characteristics grid.

be negatively affected. The solution is achieved by marching forward in time by utilizing the MacCormack finite difference scheme. At each iteration, the gas properties throughout the flowfield are updated using the JANAF polynomial given in Section 2.4. As the solution moves forward in time, all of the properties approach convergence. The outlet boundary (see Fig. 1) must be placed sufficiently far downstream of the stagnation point such that all of the flow is supersonic. This is because the solution method utilizes one-sided backwards difference equations that are only suitable in supersonic flow. As well, since this time marching finite difference solution is intended to become the input to the method of characteristics solution, it is necessary to ensure that the outlet boundary does not lie adjacent to a characteristic Mach line. At high Mach numbers the jump across the shock-wave is solved numerically using the normal shock relations and the polynomials in Section 2.4.

2.2.3. Method of characteristics (hyperbolic Euler equations)

The method of characteristics is a mathematical method that is useful in solving hyperbolic partial differential equations, such as the supersonic Euler equations. The method solves the flowfield by converting the hyperbolic PDE to a set of algebraic equations that are solved along flow characteristics. Very often, the method of characteristics can be solved assuming irrotational flow, however because the strong bow shock on a blunt body is curved, entropy and velocity gradients are created across the shock, resulting in rotational flow [8]. Thus, the rotational method of characteristics (RMOC) described by Zucrow and Hoffman was used [10]. In order to solve the rotational method of characteristics the flow is assumed to be isentropic along streamlines. For this type of flow, as described by Anderson [8] and Zucrow and Hoffman [10], three characteristic lines are required to achieve a solution to the flow field. At any point in the flow field, 4 points are selected, 3 known, and 1 unknown, forming a system of equations that is solved explicitly. The derivation of the characteristics and compatibility equations used, as well as detailed descriptions of solution processes, can be found in Zucrow and Hoffman [10].

A typical characteristics grid resulting from a calculation is shown in Fig. 2. The solution is started from an initial value line (calculated with the method in Section 2.2.2) and progressed forward in space until a desired amount of solution is achieved. The outlet of the finite difference grid and the initial value line for the RMOC solution is selected at some point ahead of the fore-body sonic line. Selecting this line closer to the sonic line is better because the RMOC solves faster and therefore slightly reduces the computation time. The characteristic equations are solved iteratively at each grid intersection. At each iteration, the JANAF polynomial given in Section 2.4 is used to update the flow properties, thus facilitating a calculation of the flow field with variable properties. When the local thermodynamics properties are updated, the local Mach angle and speed of sound change, thus impacting the downstream solution. The method of characteristics, similar to the solution to the shock-layer, is easily applied to a body shape represented by an equation. No computational grid needs to be generated or transformed. The output characteristics grid is part of the flow-field solution. In the case for bodies with regions of small radius of curvature (like that the shoulder of an atmospheric entry vehicle), in order to facilitate a solution at points along the wall, a mixture of "direct" and "inverse" wall point methods are required. In the direct wall point approach, the intersection with the wall of a Mach line emanating from a known internal flow point is calculated. However, on the aft-body it is possible that the Mach line does not intersect the body and therefore cannot be solved. In this case, a point on the wall is selected, and the data in the field is interpolated to find the point in the field where an intersecting Mach line originated. Some improvements to the author's present implementation of the method characteristics can be made, such as to allow the formation of shock-waves in the flow field.

2.3. Viscous flow

2.3.1. Integral method for laminar heating

Convective heat flux is an important design consideration in hypersonic flight. One of the most simple formulations to predict heat flux is the approach outlined by Kays et al. [11]. If the inviscid external flow properties are known, the distribution of Stanton number over a body of arbitrary shape can be easily calculated using Equation (3) [11].

$$St_x = \frac{C_1 \mu^{0.5} R G_e^{C_2}}{\left(\int_0^x G_e^{C_3} R^2 dx\right)^{0.5}} \left(\frac{T_s}{T_e}\right)^{-0.08} \left(\frac{T_{aw}}{T_e}\right)^{-0.04} \tag{3}$$

Here, $G_e = \rho_e u_e$, μ is the dynamic viscosity (evaluated at film temperature), and C_1–C_3 are empirical constants ($C_1 = 0.418$, $C_2 = 0.435$, $C_3 = 1.87$). R is the axisymmetric body radius and cancels out of the equation in the two-dimensional case as in this study. Once St_x is known, the heat flux distribution is then calculated. At the stagnation point ($x = 0$) the solution is badly behaved. This is a limitation of this method. To account for this, in the present implementation the heat flux through the stagnation region is found by linear interpolating through the badly behaved region. This typically provides smooth results that match the expected distributions.

2.3.2. Integral momentum method

A solution of the viscous boundary layer flow can be achieved by simplifying the problem by assuming a set of known similar boundary layer solutions. By integrating the boundary layer equations, and implementing boundary layer thickness parameters, the problem of the momentum flow close to the wall can be simplified to a set of ordinary differential equations [12,14]. A formulation of the integral momentum equations, and set of profile parameters for use in the solution was used in works by Lees, Reeves, and Klineberg [12,23,24]. Equations (4) to (7) were taken from Lees et al. assuming two-dimensional adiabatic flow [12]. This formulation of the boundary layer equations utilizes the Stewartson transformation of the streamwise and normal dimensions (Equation (4) and (5)). Similar equations are available for flow with heat transfer, however these are not explored here [24,13,23,12].

$$dX = \left(\frac{p_e a_e}{p_o a_o}\right) dx \tag{4}$$

$$dY = \left(\frac{a_e \rho}{a_o \rho_o}\right) dy \tag{5}$$

$$H\frac{d\delta^*}{dX} + \delta_i^* \frac{dH}{dX} + (2H+1)\frac{\delta_i^*}{M_e}\frac{dM_e}{dX} = \frac{\nu_o}{a_o M_e \delta_i^*} P \tag{6}$$

$$J\frac{d\delta^*}{dX} + \delta_i^* \frac{dJ}{dH}\frac{dH}{dX} + (3J)\frac{\delta_i^*}{M_e}\frac{dM_e}{dX} = \frac{\nu_o}{a_o M_e \delta_i^*} R \tag{7}$$

Equations (6) and (7) are the integral momentum, and moment of momentum equations, respectively. In the equations above, R, P, H and J are profile parameters that were evaluated and curve fitted to a single profile parameter a in works by Klineberg, Reeves, and Lees [12,23,24]. In these equations the parameter H is the boundary layer shape factor (not to be confused with enthalpy). In the method of Reeves and Lees [23], these equations were utilized for strong viscous-inviscid interaction and were coupled with the continuity equation (with the Prandtl–Meyer function included), to account for displacement of the external inviscid streamline. Here, the boundary layer flow is to be solved for a known Mach number distribution (calculated from an inviscid method), $\frac{dM_e}{dX}$ is known and therefore the continuity equation can be dropped and Equations (6) and (7) are the only necessary equations. A known boundary layer profile is required at the forward stagnation point in order to initialize the solution of the problem. At the stagnation point, the Cohen–Reshotko stagnation profile was utilized as the initial condition [13]. This profile is the result of a similarity solution to stagnation point flow and thus provides a reasonable estimate for an initial condition. Equations (6) and (7) were integrated downstream using the 4th order Runge–Kutta technique. The stream-wise derivatives ($\frac{d\delta^*}{dX}$ and $\frac{dH}{dX}$) were solved in a 2×2 matrix to ensure the two equations are directly coupled at each step. The solution results in a stream-wise distribution of the profile parameters R, P, H, J, and a. The shear stress is calculated from the solution by utilizing the shear stress profile parameter P which can be untransformed with Equation (8).

$$\tau_w = \mu_w \left(\frac{M_e\sqrt{\gamma R T_e}}{\delta_i^*}\right)\left(\frac{a_e \rho_w}{a_\infty \rho_\infty}\right) P \tag{8}$$

2.3.3. Numerical boundary layer solution

The compressible boundary layer equations are parabolic in nature and constitute an initial value problem. In blunt body flows, the boundary layer solution must be initialized with a stagnation point solution. Similar to the integral method in Section 2.3.2, the Cohen–Reshotko stagnation profile is used [13]. The boundary layer equations are transformed to the Levy–Lees coordinate system and are given in Equations (9)–(14) [14]. When these equations are

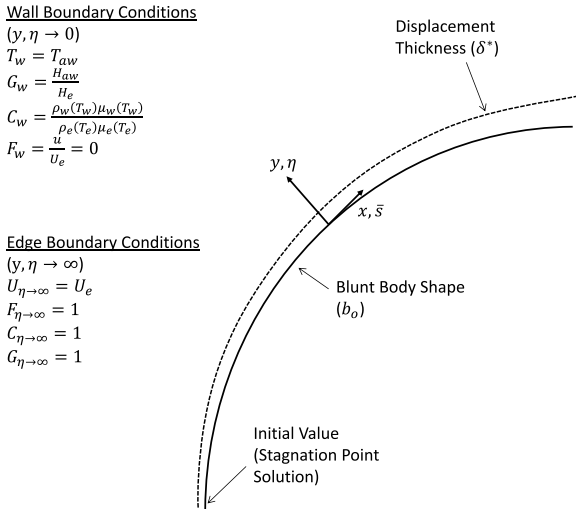

Fig. 3. Boundary layer solution set-up.

represented in the general parabolic form (Equation (15)) the system of equations is easily discretized and solved using the Crank–Nicolson method. In this form, W represents the unknown variable (F or G) and A_1 to A_4 are constants. At interior nodes the derivatives are approximated using second order central differences. First order differences are used to approximate the derivatives at the boundaries. At each stream-wise step, a tri-diagonal matrix is formulated and solved.

$$2\bar{s}F_{\bar{s}} + V' + F = 0 \tag{9}$$

$$2\bar{s}FF_{\bar{s}} + VF' = \beta\left(\frac{\rho_e}{\rho} - F^2\right) + \left(CF'\right)' \tag{10}$$

$$\begin{aligned} 2\bar{s}FG_{\bar{s}} + VG' = {} & \frac{C}{Pr}G'' + \left(\frac{C}{Pr}\right)' G' \\ & + \frac{U_e^2}{H_e}\left(\left(1 - \frac{1}{Pr}\right)\left(C'FF' + C\left(F'\right)^2 + CFF''\right)\right. \\ & \left. + CFF'\left(1 - \frac{1}{Pr}\right)'\right) \end{aligned}$$

where:

$$F = \frac{u}{U_e} \tag{11}$$

$$G = \frac{H}{H_e} \tag{12}$$

$$C = \frac{\rho\mu}{\rho_e \mu_e} \tag{13}$$

$$\beta = \frac{2\bar{s}}{U_e}\frac{dU_e}{d\bar{s}} \tag{14}$$

$$W'' + A_1 W' + A_2 W + A_3 + A_4 W_{\bar{s}} = 0 \tag{15}$$

Fig. 3 presents a diagram illustrating the boundary layer coordinate system, as well as the boundary and initial conditions. The boundary conditions for boundary layer flow are the external flow conditions (determined through solution of the inviscid flow-field) and the conditions at the wall. In this case the boundary conditions at the wall are the adiabatic wall temperature and enthalpy, as well as the no-slip condition for velocity. The Prandtl number is calculated using the thermophysical model given in Section 2.4. In order to simplify the solution, the Prandtl number was assumed to be constant at each stream-wise step thus eliminating the derivatives of Prandtl number in the normal direction. The adiabatic wall temperature gives the wall boundary condition and is

approximated using the external flow properties and Equation (20). The adiabatic wall enthalpy is calculated using the approximated wall temperature and the thermophysical model described in Section 2.4. The approximation of an adiabatic wall enthalpy simplifies the formulation of the finite difference equations by providing a Dirichlet boundary condition for G.

2.4. Thermophysical models

In high-speed flows, large gradients in temperature exist making an assumption of constant gas properties improper. In order to account for the changing gas properties throughout the flowfield, the gas properties were treated using known models. The specific heat capacity, was modeled using 7-coefficient JANAF NASA polynomials given in Equation (16) and (17) [25].

$$c_p = R_g\left(a_1 + a_2T + a_3T^2 + a_4T^3 + a_5T^4\right) \tag{16}$$

$$H = R_g\left(a_1T + a_2T^2/2 + a_3T^3/3 + a_4T^4/4 + a_5T^5/5 + a_6\right) \tag{17}$$

These polynomials were used to model nitrogen flow in the cylinder problem, and air in the leading edge problem. The polynomials closely match NIST data from 100 K to 6000 K [26].

The viscosity of the fluid was modeled using Sutherland's law. Sutherland's law for viscosity is given in Equation (18) and is valid up to 3000 K [8,27]. The modified Eucken method for thermal conductivity is given in Equation (19) [28]. The modified Eucken method is assumed to be valid as long as the calculations of c_v and μ are valid. In the previously described boundary layer models, the adiabatic wall temperature is approximated by Equation (20) from Schetz [14]. The Prandtl number is calculated with Equation (21).

$$\mu = \frac{A_sT^{3/2}}{T + T_s} \tag{18}$$

$$\kappa = \mu c_v\left(1.32 + \frac{1.77R_g}{c_v}\right) \tag{19}$$

$$T_{aw} = T_e + r\frac{U_e^2}{2c_p} = T_e + Pr^{0.5}\frac{U_e^2}{2c_p} \tag{20}$$

$$Pr = \frac{\mu c_p}{k} \tag{21}$$

3. Viscous-inviscid interaction solution

The previous sections briefly described well defined methods that on their own provide solutions to either the inviscid, or viscous flow. In reality, there is a weak viscous-inviscid interaction between the boundary layer and the external inviscid free-stream. At high Reynolds numbers, this effect can be small, but at low Reynolds numbers or cases of small radius of curvature the effect can be important. Hypersonic vehicles often operate at high altitudes where (assuming the flowfield is still a continuum) the viscous-inviscid interaction on the body can be significant. Here, a simple method where the prediction of the flow around the body is corrected for this interaction is proposed. According to Tannehill et al. [21], in general, the essential elements required to calculate a viscous-inviscid interaction are: (1) a method for obtaining the initial and improved inviscid flow solution, (2) a method for solving the boundary layer flow, and (3) a procedure for relating the inviscid and viscous flow solutions that will drive the solution to convergence. Viscous-inviscid interactions in supersonic flow have been characterized by mathematical treatment previously. Some treatments have utilized the parabolic Navier–Stokes equations [29] while others have coupled inviscid and boundary layer solutions [30–33,23,12,34]. The approach presented in this paper utilizes the latter, by solving the external inviscid flow and the boundary layer flow in an iterative fashion using the methods described in Section 2. In the present model it is assumed that the effect of the boundary layer on the external flow can be quantified by the displacement thickness (δ^*). Because the solution from the subsonic fore-body region does not join perfectly smoothly to the method of characteristics these two regions are solved separately. Initially, the inviscid solution to the shock-layer is solved for the actual body shape (b_o). The boundary layer is then solved using the conditions predicted from the inviscid solution as the edge boundary conditions that are represented by polynomial functions. The calculated displacement thickness (Equation (22)) is added to the body in the normal direction. The new body is represented by a polynomial and used to repeat the shock-layer solution. This process is repeated until convergence. Between iterations, the successive displacement of the body is calculated using the error in the displacement thickness between iterations (Equation (24)).

$$\delta^* = \int_0^\infty\left(1 - \frac{\rho u}{\rho_e u_e}\right)dy = \frac{\sqrt{2\bar{s}}}{\rho_e u_e}\int_0^\infty\left(\frac{\rho_e}{\rho} - F\right)d\eta \tag{22}$$

$$\Delta\delta_i^* = \delta_i^* - \delta_{i-1}^* \tag{23}$$

$$b_i = b_{i-1} + \Delta\delta_i^* \tag{24}$$

The above solution method was found to work well and lead to fast convergence for the subsonic forebody region, however; due to the sensitivity of supersonic flow to small perturbation in body shape, a slightly different convergence method was used for the rest of the body. Specifically, the use of the magnitude of displacement thickness as the iterative variable is not suitable. In supersonic flow the change in external streamline angle, and thus $\frac{d\delta^*}{dx}$ (displacement thickness growth), is more important in predicting stream-wise properties. Because of this, a simple convergence approach based on $\frac{d\delta^*}{dx}$ was used.

From the converged solution of the primarily subsonic portion of the fore-body, the initial boundary layer properties, and an initial value line for the method of characteristics are known. In the first iteration, a constant value of ($m = \frac{d\delta^*}{dx}$) is assumed. With this, an initial guess for the deformed body is calculated. The characteristics mesh is then evaluated using this body shape. Using the solution found from the characteristics, a new corrected body shape is determined. The error between the previous iteration's result for the profile of displacement thickness is used to predict the next iterations profile (Equations (25) to (28)). A combination of spline and polynomial fits are used in order to pass the external flow variables to the boundary layer solution, and the body shape to the inviscid solution. In order to ensure a stable solution, the streamline angle was restricted to a low order polynomial. If a spline, or direct interpolation was used, small changes in the shape of the body eventually led to divergence. This somewhat restricts the solution by smoothing out sharp changes in displaced body shape, but ensures convergence.

$$\Delta m_i = m_{calc} - m_{i-1} \tag{25}$$

$$m_i = m_{i-1} + r \times \Delta m_i \tag{26}$$

$$\delta_i^*(x) = \delta_o^* + \int m_i dx \tag{27}$$

$$b_i = b_o + \delta_i^* \tag{28}$$

An important detail of the method shown in Equations (25) to (28) is the relaxation factor r. Difficulty in convergence was present at lower Reynolds numbers. In order to stabilize the method, the iteration process is under-relaxed (typical values of r were <0.3). This is a common requirement in methods of viscous-inviscid interaction [21]. The convergence for the supersonic region of the

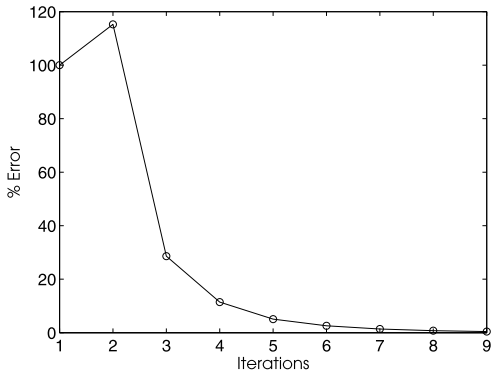

Fig. 4. Typical convergence.

flow around an adiabatic cylinder at Mach 6, and a Reynolds number of $Re = 4 \times 10^4$ is shown in Fig. 4. Here, the % error is calculated as the maximum % difference of flow properties between iterations. The result shown is typical of other test cases examined.

4. CFD simulations

4.1. Solver and setup

Hypersonic flow over an adiabatic circular cylinder and a cooled blunt leading edge were used as test cases in this study. High-fidelity simulations performed by the present authors as part of related studies have been used for comparison to the simplified methods described in the previous sections [1,16]. In both of these cases, rigorous mesh independence studies have been performed. In [16], the adiabatic cylinder case has been compared to experimental synthetic Schlieren images, and pressure distributions. In those studies a full description of their respective set-up and validation can be found. In the present work these simulation results are to be used as the bench-mark for calculation accuracy and set-up of these simulations is only briefly covered.

Simulations were performed using the open-source CFD software OpenFOAM version 2.3.0 [15]. In particular, the density based compressible flow solver, rhoCentralFoam, was used [19]. The simulations were performed assuming continuum, equilibrium, and laminar flow. The thermophysical modelling implemented in the solver are the Sutherland, and JANAF models described in Section 2.4. The governing equations solved in rhoCentralFoam are the compressible Navier–Stokes equations (Equations (29) to (31)) [19].

$$\frac{\partial \rho}{\partial t} + \nabla \cdot (\rho u) = 0 \tag{29}$$

$$\frac{\partial (\rho u)}{\partial t} + \nabla \cdot u(\rho u) - \nabla p - \nabla \cdot \tau = 0 \tag{30}$$

$$\frac{\partial \rho E}{\partial t} + \nabla \cdot (u(\rho E)) + \nabla \cdot [up] + \nabla \cdot (\tau \cdot u) + \nabla \cdot j = 0 \tag{31}$$

where ρ, u, p, j, τ, and E represent the density, velocity, pressure, diffusive heat flux, viscous stress tensor, and total energy respectively. RhoCentralFoam has been used previously by the present authors and shown good results with comparison to experiment and other CFD packages [35,36,1,17,18].

In both the adiabatic circular cylinder and cooled leading edge test cases the simulations were performed on grids consisting entirely of unstructured hexahedral elements. The inlet boundary conditions were set with constant p, T, and u. The outlet, as well as the top and bottom boundaries were all treated as zero-gradient for all properties. Free-stream properties such as Mach number, Reynolds number, and dynamic pressure of the flow were controlled through manipulation of the inlet pressure, temperature and velocity.

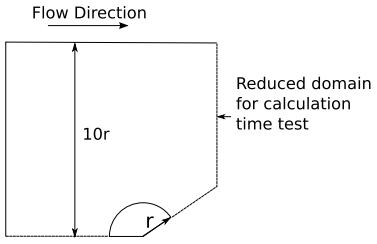

Fig. 5. Domain for full cylinder simulations.

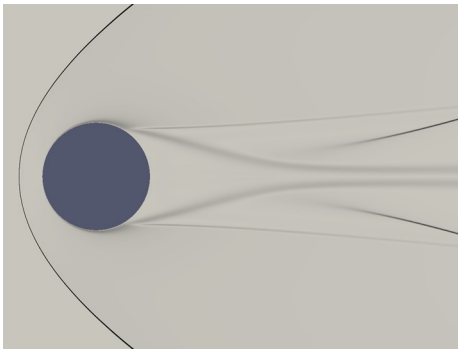

Fig. 6. Typical CFD result (synthetic Schlieren, $M = 6$, $Re = 40000$).

4.2. Test case: adiabatic circular cylinder

The primary goal of the adiabatic cylinder cases is to examine the ability of the investigated methods to predict the distributions of pressure and friction forces. Additionally the effect of Reynolds number on the effectiveness of the methods (particularly the interaction model) is of interest. The test gas in this study was nitrogen. A schematic of the domain is shown in Fig. 5. Full details of these simulations can be found in related work [16]. The domain was sized to ensure that no boundary interference effects were present in the results. A typical simulation result is shown by a synthetic Schlieren image in Fig. 6. To compare the solution time of full CFD and the simplified methods, additional simulations were performed with a reduced domain. In these cases the outlet was set at 125° and a symmetry plane was used to reduce the domain size. The reduced domain is depicted in Fig. 5.

4.3. Test case: cooled leading edge

The primary goal of the cooled leading edge cases is to evaluate the ability of the investigated methods to capture convective heat flux distributions in hypersonic flow. In these cases, Mach 10 flow at a free-stream dynamic pressure of $q_\infty = 9.57604 \times 10^4$ Pa and free-stream static temperature of 225 K is simulated over blunt leading edges with a constant wall temperature ($T_w = 311.1$ K). The test gas in this case was air. These properties were chosen to simulate flight at approximately 29 km. Because of the cold wall, significant heat flux is transfered to the edge. Two different leading edge geometries are examined. Geometry 1 has sharp shoulders and a high radius of curvature near the stagnation region. Geometry 2 is a hemicylindrical geometry. In Fig. 7 the geometries and their respective simulation domains are shown. The domain was sized to allow the bow shock to exit the simulation through the outlet and not reflect off the top and bottom. Full details regarding the design of these simulations can be found in the related work [1].

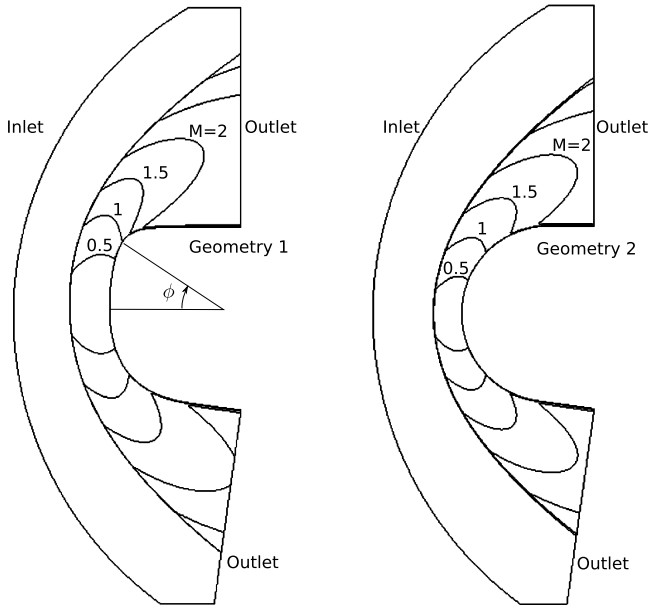

Fig. 7. Simulation geometry with associated Mach number isolines.

Simulation of stagnation point heating requires special consideration in terms of grid generation. The computational grid was generated using the native OpenFOAM meshing utility blockMesh. The grid employs shock alignment to capture the bow-shock and high grid resolution in the boundary layer. The cell Reynolds number at the stagnation point was ensured to meet the criteria of $Re_c < 5$ [37]. These extra considerations required for accurate results increase the cost of each simulation by increasing the number of cells and the time spent generating each grid.

Typical simulation results are depicted by Mach isolines in Fig. 7. Because of the difference of results (rate of flow acceleration, standoff distance etc.) these two geometries provide adequate test cases for the low and intermediate fidelity solvers.

5. Results and discussion

5.1. Pressure distribution – adiabatic circular cylinder

The modified Newtonian method is known to give good results for pressure distribution close to the stagnation point on the fore-body. This is confirmed in Fig. 8 at a representative Reynolds number (Re = 20000). The coefficient of pressure (see Equation (2)) is shown from 0 to 120 degrees from the forward stagnation point. Up to approximately 50 degrees the modified Newtonian theory shows close agreement to the other methods. Past this point it can be seen that Newtonian theory begins to diverge significantly from the other solutions.

The ability to predict flow past the shoulder (aft-body) is important for finite bluff bodies such as re-entry vehicles. The pressure distributions past 60 degrees are normalized to the predicted stagnation pressure at the fore-body stagnation point. Fig. 9 shows the results for three representative Reynolds numbers. Close agreement is visible between the laminar Navier–Stokes simulation (rhoCentralFoam) and the SFFD and the RMOC with interaction up to 120° for three Reynolds numbers. The results of the SFFD and the RMOC without interaction still show close results to the CFD solution. In the high Reynolds number case, it is clear that less advantage was gained in prediction of the pressure distribution by accounting for the interaction. At a Reynolds number of $Re = 8000$, the change in the pressure distribution due to the viscous interaction calculation is noticeable. The poor performance of the modified Newtonian theory in this region is evident.

A summary of the effect of Reynolds number, and the relative accuracy of each method is shown in Fig. 10. The plot shows the maximum percent error in normalized pressure between 0 and 110 degrees. The % error is calculated between the predicted and the rhoCentralFoam results. It is clear that over the Reynolds number range investigated, the correction for viscous interaction leads to a significant improvement in accuracy for the prediction of pressure distribution. At a Reynolds number of $Re = 8000$, the error reduced from approximately 50% to 10% when the solution to the SFFD and RMOC solution was corrected for the viscous-inviscid interaction. At a Reynolds number of $Re = 80000$ the reduction in error is less significant but still yields improved accuracy. This justifies the use of the present method of correction throughout the investigated Reynolds number range. The Newtonian method has large error and only mildly increases in accuracy with Reynolds number. The SFFD and RMOC solution gives more accurate results than the Newtonian method, and the error reduces noticeably with increasing Reynolds number.

5.2. Shear stress – adiabatic circular cylinder

To assess the accuracy and applicability of the boundary layer methods described in Section 2.3, the shear stress was compared along the surface of the adiabatic cylinder. In Fig. 11, the coefficient of friction $c_f = \frac{\tau_w}{0.5\rho_\infty U_\infty^2}$ is plotted as a function of angle from the forward stagnation point. The results were compared for different combinations of inviscid and viscous solutions, as well as with and without the interaction method presented in Section 3. The results for shear stress lead to similar conclusions regarding the applicability of the methods as the results for pressure distribution. Variations in the external flow properties influence the development of the boundary layer. Therefore the quality of the

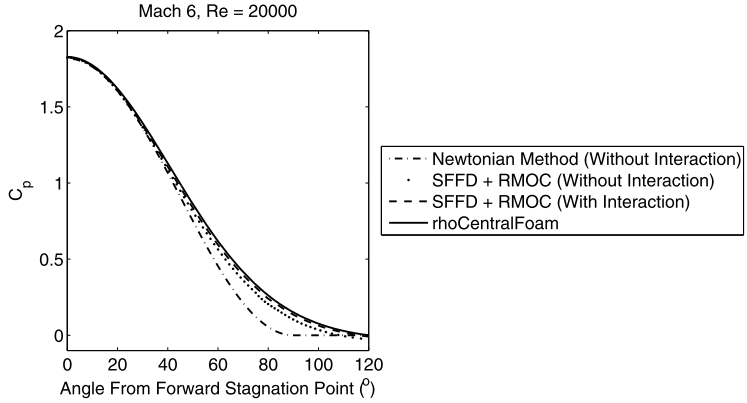

Fig. 8. Pressure distribution.

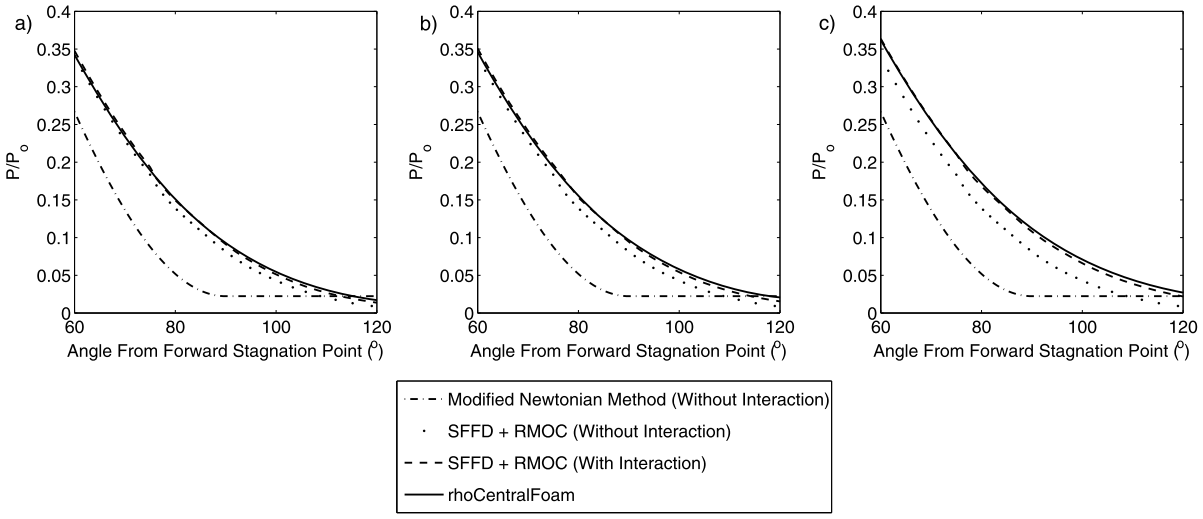

Fig. 9. Pressure distribution a) $Re_\infty = 80000$, b) $Re_\infty = 40000$, c) $Re_\infty = 8000$.

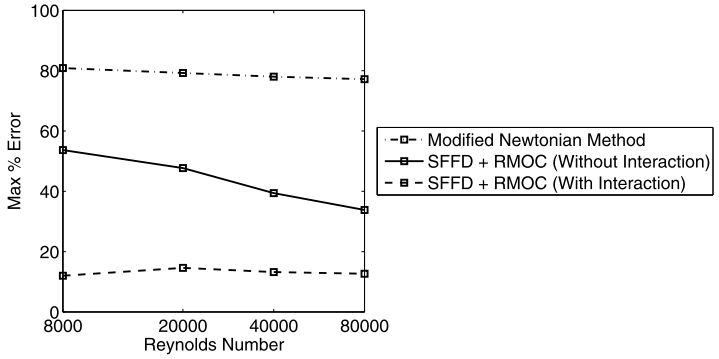

Fig. 10. Max % error in normalized pressure (P/P_o).

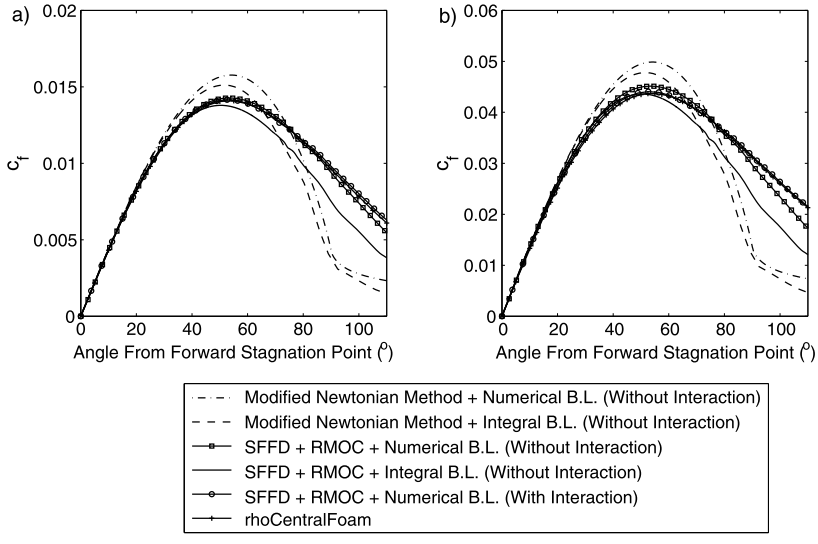

Fig. 11. Coefficient of friction a) $Re_\infty = 80000$, b) $Re_\infty = 8000$.

boundary layer solution is not only a function of the applicability of the assumptions in the governing equations, but also by the quality of the solution for the boundary conditions (p_e, U_e, M_e, T_e, T_{aw} and μ_w). Using the Newtonian method (along with isentropic flow relations) for the external flow parameters, the results from the integral momentum method, and the numerical solution of the compressible boundary layer equations were relatively poor. The results show that the correct shape for the shear stress profile are found; however the magnitude of the peak coefficient of friction is over-predicted. The maximum calculated error between the Newtonian method boundary layer predictions was for the integral momentum method. Past 90°, where the pressure is assumed constant, the solution shows especially poor results.

Using the solutions based on the SFFD and RMOC to give the external flow parameters, all of the results show improved agreement to the CFD. The solution given by the integral momentum

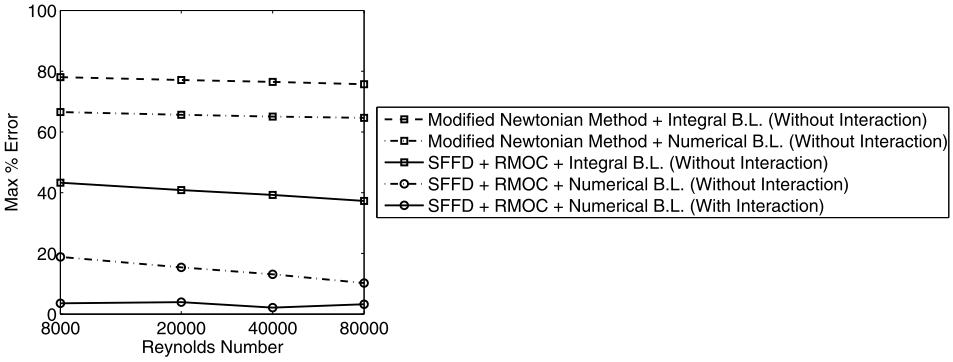

Fig. 12. Max % error in coefficient of friction (C_f).

method shows an improvement from the Newtonian method for the distribution of shear stress, however the magnitude of c_f is under-predicted, particularly on the aft-body. The reduced accuracy of the integral method is due to the restriction of the solution to a family of boundary layer profiles, in this case the Klineberg [24] polynomials. The SFFD and RMOC solution to the inviscid flow, with the numerical solution of the boundary layer equations shows good results for shear stress distribution along the body. The predictions match closely up to 90 degrees but have increasing error on the aft-body. This is because as the flow expands around the cylinder, the favorable pressure gradient induces boundary layer growth, which then acts to alter the pressure distribution. This can also be seen in the pressure distribution results previously discussed. As the Reynolds number is increased this effect reduces in importance and the accuracy of this method improves greatly. The improvement of the solution by implementing the weak interaction correction given in Section 3 is seen in the results for shear stress. The corrected shear stress closely matches the CFD results in all cases. A summary of the accuracy of each method in the Reynolds number range investigated is shown in Fig. 12. The maximum % error in coefficient of friction between 0 and 110 degrees is plotted. The % error is calculated between the predicted and the rhoCentralFoam results. The increased accuracy of the numerical boundary layer solution is evident. For the present method, the error in coefficient of friction is $< 10\%$ throughout the range of Reynolds numbers investigated. Because of the increased accuracy at higher Reynolds numbers of the simulation without the interaction solution, the gains in accuracy due to the inclusion of this model are reduced as Reynolds number is increased. At the lowest Reynolds number the gain in accuracy is much more noticeable.

5.3. Heat flux – cooled leading edge

For the cooled leading edge, only the Kays et al. [11] method for laminar heating, and the numerical solution to the boundary layer equations were used to analyze the viscous part of the flow. The momentum integral approach was not used for the heat flux study because Equations (6) and (7) (as they are written) along with the family of boundary layer profiles used are only valid for an adiabatic wall problem. The equations can be altered to include the energy equation, and a family of profiles accounting for heat flux [24] but this is not done in the present work. The modified Newtonian method and the shock fitted finite difference grid were used for the inviscid flow. Neither the method of characteristics or the interaction correction were implemented for this case. The primary reason for examining those methods was to capture the shoulder region expansion which does not occur on these leading edges.

The heat flux distributions for the cooled leading edges shown in Fig. 7 are plotted in Fig. 13. From the results, the modified Newtonian theory with the Kays et al. [11] laminar heating model over-predicts the peak heat flux for both geometries. Additionally, this approach over-predicts the sensitivity of the heat flux distribution to changes in geometry. This weakness can be important in the design of aero-thermal components. When the Kays et al. [11] laminar heating model was used with the SFFD solution for an inviscid input the peak heat flux was under-predicted but the shape of the distribution was more correct.

As expected, the combination of the numerical boundary layer solution with the SFFD solution provides the best result. Both the magnitude and shape of the heat flux distribution are in close agreement. For the simpler shape (geometry 2) where the radius of curvature is nearly constant the results are almost identical. The more complicated geometry resulted in more error however the results still agree closely.

5.4. Relative accuracy and computing time

The adiabatic circular cylinder problem was used to characterize the relative accuracy and computing time. Additional simulations were performed with a reduced domain at the highest Reynolds number investigated here ($\mathrm{Re} = 80000$). The goal of these simulations was to compare the relative accuracy and computing time of each of the simplified methods in comparison to CFD solutions of varying resolution. The domain was reduced in order to give a fair representation of the simulation time of rhoCentralFoam (see Fig. 5). In the previous section the entire flow solution was achieved and thus the simulation time was much longer and could not be compared to the time required for the simplified calculations. In Fig. 14, the relative accuracy compared to computation time is shown. Both the error and the calculation time are normalized to the error and calculation time of the most simple method (modified Newtonian method + integral boundary layer). This way the penalties in cost and accuracy can more easily be visualized as multiples of each other. The specific values in seconds or hours would be heavily influenced by computer speed and efficiency of programming. By normalizing the values this problem is reduced because all of the simplified codes were written by the same author and all simulations were computed on the same computer system.

The grids were refined by doubling the number of cells in both principal directions. Thus the fine grid has 4 times and 16 times as many cells as the medium and course grids, respectively. The grid convergence index based on peak shear stress was 1.53 from the coarse to medium grids, and 0.33 from the medium to fine grids. The results in Fig. 14 contain an important observation regarding the use of CFD with insufficient grid resolution. Despite the fact that full CFD does not simplify the equations in any way, when insufficient grid resolution is used the results are less accurate than the simplified methods and in fact take more time.

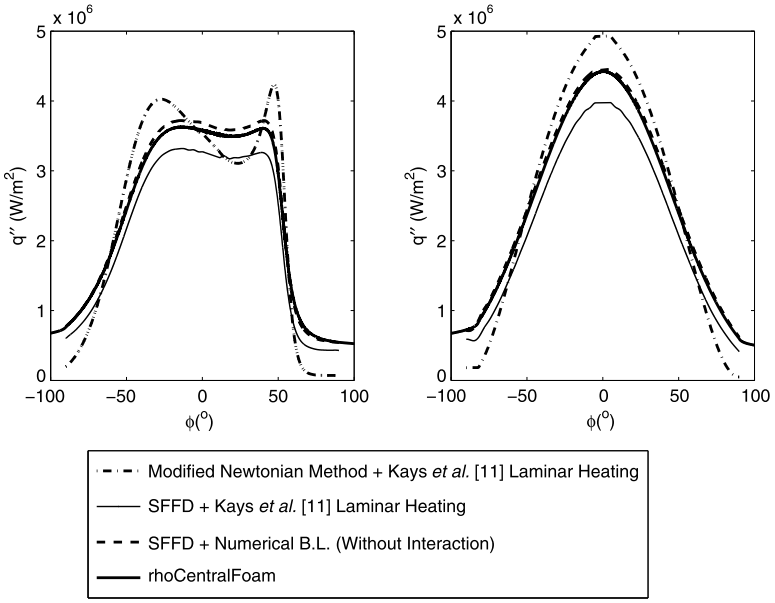

Fig. 13. Heat flux distributions – (left) geometry 1 (right) geometry 2.

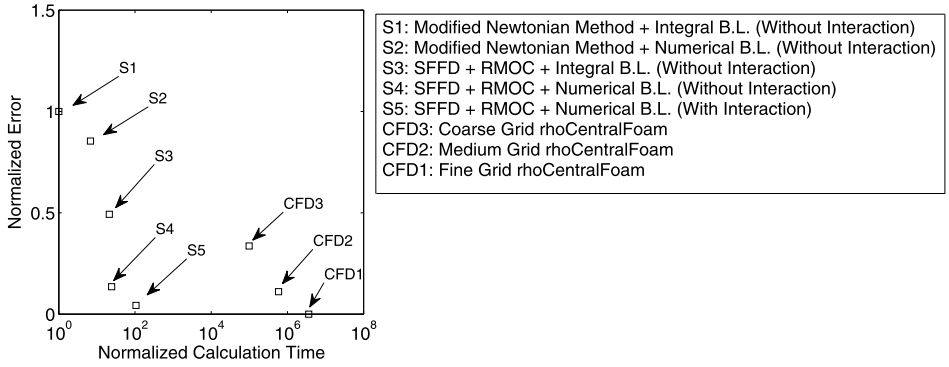

Fig. 14. Normalized error (in shear stress) and computation time (M = 6, Re = 80000).

For example, the present method here that includes a correction for viscous-inviscid interaction (Section 3) is nearly four orders of magnitude faster than the medium resolution CFD simulation and produces more accurate results. Additionally the computation time was nearly 5 orders of magnitude faster than the fine grid solution. It is difficult to know ahead of time whether a single CFD grid setup will be of sufficient resolution throughout an entire design space. Therefore an engineer has the choice of choosing an extremely high grid resolution to increase confidence, or choose a moderate grid refinement and hope that the resulting error is insignificant. This is a major obstacle and makes a strong case for using simplified numerical methods for rapid calculations. It is therefore easy to see the benefit of using a carefully selected and designed simplified numerical approach. In the design space for a blunt hypersonic body such as a leading edge or heat shield the simplified methods could construct a superior surrogate model based on significantly more samples requiring fewer CFD simulations, or even be used directly to perform the optimization. In previous work by the present authors, methods of varying fidelity were used in sequence to narrow the design space and then approach the optimal result [1].

Aside from computational cost and accuracy there are also important concerns regarding front-end costs. For example, commercial software such as OpenFOAM or FLUENT can have added front-end costs such as steep learning curves or licensing costs. Alternatively, unlike a commercial software, the code for these simplified methods typically doesn't exist and therefore must be developed. Certain methods such as the Newtonian method are extremely simple and require negligible time to implement. However a more complicated method such as the present method took appreciable time and testing. This can be a strong argument against simplified methods in circumstances where front-end time is extremely valuable and results are needed right away. In the long term it can often be worth it to develop these codes. Some simplified codes that have been effectively used for design are XFoil for airfoils [38], or CBAero for hypersonic flight vehicles [39,40]. For the present authors, all of the methods described in Section 2 and 3 have been combined into a tool named HyPE2D which has recently been used for the optimization of blunt leading edges for wave-riders [1].

6. Conclusion

Simple analytical and numerical methods were used to analyze two hypersonic blunt body flow problems. A simple method for accounting for the weak viscous-inviscid interaction between the boundary layer and the external free-stream was given. The results were compared to those obtained from the numerical simulation of the compressible Navier–Stokes equations. The analysis was performed in the context of evaluating each methods merits to be used for the rapid design and analysis of hypersonic blunt bodies. The results showed that a specific surface inclination method (the

modified Newtonian method, Section 2.2.1) has limited applicability because of its poor accuracy away from the forward stagnation point. A solution to the Euler equations using a shock-fitted finite difference grid (Section 2.2.2) combined with the method of characteristics (Section 2.2.3) showed close agreement but reduced in accuracy at lower Reynolds numbers. A good approximation of the convective heat flux distribution was achieved using a simple integral calculation (Section 2.3.1). The integral boundary layer method (Section 2.3.2) utilizing a single parameter family of profiles was found to under predict the shear stress around the body. The numerical solution to the compressible boundary layer equations (Section 2.3.3) showed close agreement to the CFD results for both shear stress and convective heat flux. The results from the simple viscous-inviscid interaction solution (Section 3) showed improved accuracy from the calculations where the interaction was ignored, particularly at low Reynolds numbers. The relative accuracy and computing time of each method was compared to a series of CFD simulations with reduced grid refinements. It was shown that an under-resolved CFD simulation can result in significantly reduced accuracy and still take several orders of magnitude longer to compute than lower order models.

Conflict of interest statement

No conflict of interest to declare.

Acknowledgements

This research was enabled in part by support provided by WestGrid (www.westgrid.ca) and Compute Canada Calcul Canada (www.computecanada.ca). Financial support was provided by the Natural Sciences and Engineering Research Council of Canada (NSERC).

References

[1] W.S. Hinman, S. Schmitt, C.T. Johansen, P.E. Rodi, Computational fluid dynamics study of optimized hypersonic leading edge geometries, AIAA Paper 2015-2509, July 2015.
[2] P.E. Rodi, Optimization of Bezier curves for high speed leading edge geometries, AIAA Paper 2013-1004, January 2013.
[3] P.E. Rodi, Integration of optimized leading edge geometries onto waverider configurations, AIAA Paper 2015-1700, January 2015.
[4] P.J. Roache, Quantification of uncertainty in computational fluid dynamics, Annu. Rev. Fluid Mech. 29 (1) (1997) 123–160.
[5] N.V. Queipo, R.T. Haftka, W. Shyy, T. Goel, R. Vaidyanathan, P. Kevin Tucker, Surrogate-based analysis and optimization, Prog. Aerosp. Sci. 41 (1) (2005) 1–28.
[6] A.I.J. Forrester, A. Sóbester, A.J. Keane, Multi-fidelity optimization via surrogate modelling, Proc. R. Soc., Math. Phys. Eng. Sci. 463 (2088) (2007) 3251–3269.
[7] A.I. Forrester, A.J. Keane, Recent advances in surrogate-based optimization, Prog. Aerosp. Sci. 45 (1–3) (2009) 50–79.
[8] J.D. Anderson, Hypersonic and High-Temperature Gas Dynamics, 2nd ed., AIAA, Blacksburg, Virginia, 2006.
[9] M.D. Salas, A Shock-Fitting Primer, Taylor & Francis Group LLC, Boca Raton, FL, 2010.
[10] M.J. Zucrow, J.D. Hoffman, Gas Dynamics, vol. 2, John Wiley and Sons, 1977.
[11] W. Kays, M. Crawford, B. Weigand, Convective Heat and Mass Transfer, 4th ed., McGraw-Hill, New York, NY, 2005.
[12] L. Lees, B.L. Reeves, Supersonic separated and reattaching laminar flows: I. General theory and application to adiabatic boundary-layer/shock-wave interactions, AIAA J. 2 (11) (1964) 1907–1920.
[13] C. Cohen, E. Reshotko, Similar solutions for the compressible laminar boundary layer with heat transfer and pressure gradient, 1956, NACA TR 1293.
[14] J.A. Schetz, Boundary Layer Analysis, 1st ed., Prentice Hall, Upper Saddle River, New Jersey, 1993.
[15] OpenFOAM, OpenCFD Ltd, 2015.
[16] W.S. Hinman, C.T. Johansen, Interaction theory of hypersonic laminar near-wake flow behind an adiabatic circular cylinder, Shock Waves (2015), http://dx.doi.org/10.1007/s00193-015-0615-y.
[17] C. Arisman, C.T. Johansen, Nitric oxide chemistry effects in hypersonic boundary layers, AIAA J. 53 (12) (2015) 3652–3660.
[18] C. Arisman, C.T. Johansen, B. Bathel, P. Danehy, Investigation of gas seeding for planar laser-induced fluorescence in hypersonic boundary layers, AIAA J. 53 (12) (2015) 3637–3651.
[19] C.J. Greenshields, H.G. Weller, L. Gasparini, J.M. Reese, Implementation of semi-discrete, non-staggered central schemes in a colocated, polyhedral, finite volume framework, for high-speed viscous flows, Int. J. Numer. Methods Fluids 63 (1) (2009) 1–21.
[20] J.F. McCarthy, T. Kubota, A study of wakes behind a circular cylinder at M equal 5.7, AIAA J. 2 (4) (Apr 1964) 629–636.
[21] J.C. Tannehill, D.A. Anderson, R.H. Pletcher, Computational Fluid Mechanics and Heat Transfer, 2nd ed., Taylor & Francis, 1997.
[22] J. Cousteix, J. Mauss, High Reynolds number flows, in: Asymptotic Analysis and Boundary Layers, 1st ed., Springer, Verlag, Berlin, Heidelberg, 2007, pp. 133–158.
[23] B.L. Reeves, L. Lees, Theory of laminar near wake of blunt bodies in hypersonic flow, AIAA J. 3 (11) (1965) 2061–2074.
[24] J.M. Klineberg, L. Lees, Theory of laminar viscous-inviscid interactions in supersonic flow, AIAA J. 7 (12) (1969) 2211–2221.
[25] J. Mcbride, A. Reno, Coefficients thermodynamic properties for calculating and transport of individual species, 1993, NASA-TM-4513.
[26] NIST-JANAF Thermochemical Tables, http://kinetics.nist.gov/janaf/ [Online Database].
[27] E. Rathakrishnan, Theoretical Aerodynamics, 1st ed., John Wiley & Sons Singapore Pte. Ltd., Singapore, 2013.
[28] B.E. Poling, J.M. Prausnitz, J.P. O'Connell, Thermal conductivity, in: The Properties of Gases and Liquids, 5th ed., McGraw-Hill, New York, 2001, pp. 10.1–10.70, chap. 10.
[29] M. Barnett, R.T. Davis, Calculation of supersonic flows with strong viscous-inviscid interaction, AIAA J. 24 (12) (Dec 1986) 1949–1955.
[30] E.D. Doss, H.A. Dwyer, A. Goldman, Rapid calculation of inviscid and viscous flow over arbitrary shaped bodies, J. Aircr. 8 (2) (Feb 1971) 125–127.
[31] T.A. Reyhner, T.E. Hickcox, Combined viscous-inviscid analysis of supersonic inlet flowfields, J. Aircr. 9 (8) (Aug 1972) 589–595.
[32] W. Johnston, P. Sockolf, Matching procedure for viscous-inviscid interactive calculations, AIAA J. 17 (6) (jun 1979) 661–663.
[33] J.-M. Grange, J.M. Klineberg, L. Lees, Laminar boundary-layer separation and near-wake flow for a smooth blunt body at supersonic and hypersonic speeds, AIAA J. 5 (6) (1967) 1089–1096.
[34] G. Miller, Mathematical formulation of viscous-invsicid interaction problems in supersonic flow, AIAA J. 11 (7) (1973) 938–942.
[35] W.S. Hinman, C.T. Johansen, Numerical investigation of laminar near wake separation on circular cylinders at supersonic velocities, in: 29th Congress of the International Council of the Aeronautical Sciences, International Council of the Aeronautical Sciences, St. Petersburg, Russia, 2014, pp. 1–10.
[36] W.S. Hinman, C.T. Johansen, S.J. Wilson, Application of simplified numerical and analytical methods for rapid analysis in atmospheric entry vehicle design, AIAA Paper 2015-0030, January 2015, 2015.
[37] P. Papadopoulos, E. Venkatapathy, D. Prabhu, M.P. Loomis, D. Olynick, Current grid-generation strategies and future requirements in hypersonic vehicle design, analysis and testing, Appl. Math. Model. 23 (9) (1999) 705–735.
[38] M. Drela, XFOIL: an analysis and design system for low Reynolds number airfoils, in: Low Reynolds Number Aerodynamics, Springer, 1989, pp. 1–12.
[39] D. Kinney, Aero-thermodynamics for conceptual design, AIAA Paper 2004-31, January 2004.
[40] D. Kinney, Aerothermal anchoring of CBAERO using high fidelity CFD, AIAA Paper 2007-608 January 2007.